Numerical Flow Simulation of a Natural Gas Engine Equipped with an Unscavanged Auto-Ignition Prechamber

D. Wunsch[1], S. Heyne[*, 1], J.B. Vos[2], D. Favrat[1]

[1] École Polytechnique Fédérale de Lausanne (EPFL), Switzerland
[2] CFS Engineering, Scientific Park Lausanne, Switzerland

Abstract
A three-dimensional Reynolds-Averaged Navier-Stokes (RANS) simulation was carried out on an unscavanged auto-ignition prechamber-cylinder configuration in order to understand better the ignition conditions inside the engine. The sensitivity to different boundary conditions like initial gas and wall temperature was tested and flow simulations coupled with a 55 species chemical mechanism were carried out in order to determine the starting location of auto-ignition. It was shown that the initial gas temperature has the greatest influence on the ignition timing and that there still is a high risk of premature ignition inside the main chamber with the current prechamber design.

Introduction

This work was undertaken as part of on-going research at the Industrial Energy Systems Laboratory (LENI) on stationary natural gas (co-generation) engines equipped with ignition prechambers. Successful operation of engines with spark-ignited prechambers has been demonstrated for both natural gas and biogas [1-3]. A major advantage of this system is that the stringent Swiss emission regulations [4] may be met without catalytic post-treatment of the exhaust gases, while still achieving good thermal efficiencies. This is of particular importance in the case of biogas, where use of a catalyst would require costly gas pre-treatment.

A new approach has been pursued at LENI in order to trigger homogeneous auto-ignition inside the prechamber, similar to HCCI. Ignition inside the pre-chamber is promoted by resistive heating of the upper prechamber part. This contrasts with previous works [5 - 8] where prechamber ignition was achieved by direct injection into the prechamber, or with a spark or glow plug ignition system, all requiring relatively large prechambers. Potential advantages of the new system include greater service intervals since there is no need to replace spark plugs. Lower emissions of carbon monoxide and unburned hydrocarbons are anticipated because, compared to a spark ignited prechamber, the auto-ignition prechamber design gives a faster transfer of the flame from the prechamber into the main chamber. Furthermore, homogeneous ignition avoids the initial expulsion of cold, un-reacted gas from the prechamber, which reduces the necessary volume of the prechamber for equivalent ignition performance. The heated auto-ignition prechamber design has been installed on an experimental single-cylinder engine at LENI. Its specifications are given in Table 1 and a schematic drawing of the prechamber setup is shown in Fig. 1.

Table 1
Engine operation parameters

Bore [mm]	95.25
Stroke [mm]	114.3
Piston rod length [mm]	222.25
Compression ratio ε	13
RPM [min^{-1}]	1500
Relative air-to-fuel ratio λ	1.3

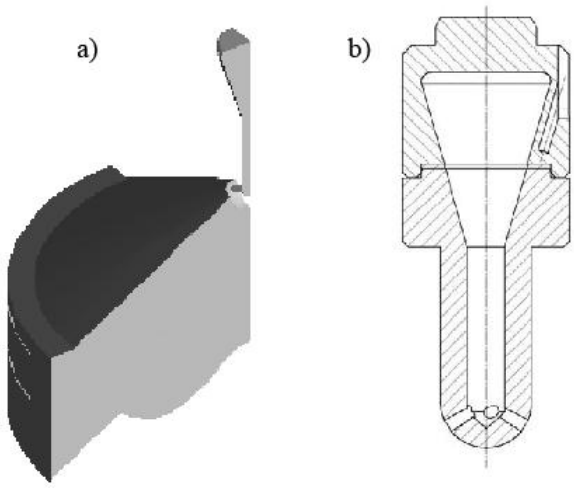

Fig. 1: Prechamber setup: a) View of a quarter of the computation domain of the engine with prechamber, b) detailed view of the prechamber.

By simulation of a direct injection engine, Zheng et al. [5] demonstrated the dependence of engine performance on injection timing, natural gas composition and initial temperature. Crane and King [6] tested different prechamber designs for lean-premixed natural gas engines with additional direct injection into the prechamber. They showed that a staged prechamber could extend the lean operation limit up to $\lambda = 1.82$ (equivalence ratio $\phi = 0.55$) and reduce both the NO_x

[*] Corresponding author: stefan.heyne@epfl.ch
EPFL / LENI-ISE-STI, Bat. ME A 2, Station 9, 1015 Lausanne, Switzerland; http://leni.epfl.ch
Proceedings of the European Combustion Meeting 2007

and HC emissions compared to standard spark ignition. The Bowl-Prechamber-Ignition concept of Kettner et al. [7, 8] also displayed reduced NO_x emissions and reduced knock sensitivity.

Due to the difficulty of gaining optical access into the single-cylinder engine at LENI, the ignition event was studied using numerical simulation for the most promising operating condition, 1500 rpm with a relative air-to-fuel ratio of $\lambda = 1.3$. The location of the earliest auto-ignition event is of primary interest.

Specific Objectives

The boundary and initial conditions for the simulation were based on measured data where available. The initial gas composition was obtained from a gas component analysis and the temperature was evaluated using the ideal gas law. The composition was assumed to contain CH_4, C_2H_6, C_3H_8, CO_2 and N_2 only. The small amounts of higher order carbon compounds were neglected, as natural gas and its ignition characteristics are sufficiently well represented by the C_1 to C_3 components [9]. The gas temperature at 180 °CA BTDC and an averaged gas temperature over an entire cycle were needed as an initial condition and for the heat flux analysis respectively. The cylinder wall and head temperature were assumed constant over an engine cycle and were calculated by a heat flux analysis using the measured cooling water flow. The prechamber wall temperature was measured in its heated upper part. A conduction analysis for the prechamber wall showed a virtually constant prechamber wall temperature, also for the part which is not heated. The initial mixture composition was calculated based on the known gas composition and an air-to-fuel ratio λ of 1.3 for all simulations. The mixture was assumed to be homogeneous in both the main chamber and prechamber. This represents a simplification as the residual gas concentration is expected to be higher in the prechamber compared to the main chamber after the intake stroke. The base case initial and boundary conditions are given in Table 2

Table 2
Initial and boundary conditions for the base case (at bottom dead centre ≙ 180 °CA BTDC)

Initial gas temperature [K]	460.3
Initial pressure [bar]	1.099
Cylinder wall temperature [K]	376
Cylinder head temperature [K]	376
Prechamber wall temperature [K]	793.2
Gas composition [mole fractions]	
CH_4	0.0677
C_2H_6	$3.065 \cdot 10^{-3}$
C_3H_8	$6.964 \cdot 10^{-4}$
CO_2	$6.964 \cdot 10^{-4}$
O_2	0.1945
N_2	0.7333

For a compression ratio of 13 a mesh was generated - using ICEMCFD - for the use with the Multi-Block Navier-Stokes solver NSMB [10]. The calculations were performed from 180 °CA BTDC to 180 °CA ATDC. The valves were disregarded in the geometric model; therefore it was assumed that they were closed during the compression and expansion strokes. This represent a simplification, since in reality the intake valve is closed 130 °CA before top dead center. However, this simplification should be acceptable in comparison to the uncertainties of the other properties that had to be predicted. In addition it has the great advantage of rendering the geometry symmetrical reducing the 3-D simulation to a quarter of the cylinder. The piston motion is described by a slider-crank-model and an arbitrary Lagrangian-Eulerian (ALE) approach is used for the dynamic mesh deformation. No cells are eliminated during mesh compression. This allows a coarser meshing of the main chamber as the cell size is reduced during compression. The reference mesh shown in figure 2 consists of 86 blocks with an overall number of 247763 hexahedral cells.

The spatial discretization in NSMB is done by a central finite volume method and the temporal discretization used for the simulations is a dual time stepping with 2nd order implicit backwards scheme for the outer time steps and multiple Gauss-Seidel iterations for the quasi-steady state solution in the inner time step. The turbulence model used for the calculations is the one-equation Spalart-Allmaras model. The data output used for the simulations was 0.5 ms corresponding to 4.5° CA at 1500 rpm. This is not an optimal resolution but was chosen due to calculation time limitations.

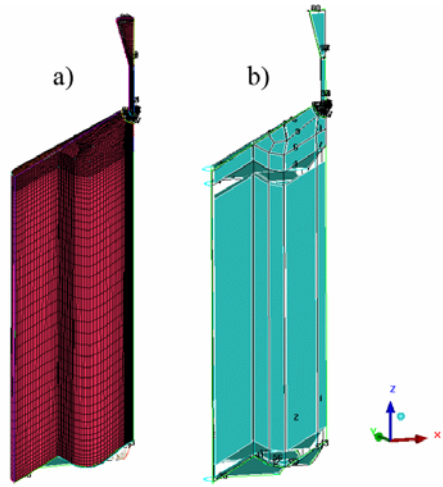

Fig. 2: Simulation domain for the prechamber configuration: a) mesh, b) blocking.

A sensitivity analysis was performed modifying the base case. The following properties were varied in order to determine their influence and to find the time and place of first ignition:

- The cylinder wall and head temperature
- The prechamber wall temperature
- The initial gas temperature.

A final simulation was then conducted based on an experimental case.

Simulations of the inert flow field without chemistry were conducted and evaluated, assuming that the chemical reactions before first ignition do not influence the flow field significantly. This allowed the detection of the hot spots prone to ignition. Then the evaluation was extended taking the chemical part into account by following two different approaches: The first approach involved selecting a number of cells covering the most interesting regions and adding the chemical heat release into the inert flow field calculation. The chemical evolution of these cells, subject to the modified temperature and pressure was modelled using the Senkin module of the CHEMKIN II package [11]. The contribution of the reaction energy on the pressure and temperature is taken into account as an additive term for the temperature increase. The pressure is corrected based on an adiabatic compression related to the new temperature.

$$T_{n+1} = \underbrace{T_{n+1,Senkin}}_{\substack{chemical\\contribution}} + \underbrace{(T_{n+1,CFD} - T_{n,CFD})}_{\substack{fluid\ dynamics\\contribution}} \tag{1}$$

$$P_{n+1} = P_n \cdot \left(\frac{T_{n+1}}{T_{n,CFD}} \right)^{\frac{\gamma}{\gamma-1}} \tag{2}$$

in which the temperature T, the pressure P and the adiabatic coefficient γ, n indexing the corresponding time step and *Senkin* respectively *CFD* the source for the temperature. The ignition criterion used was a steep increase in the OH radical concentration. This approach allowed an efficient comparison of the different simulated cases; however the location of first ignition is limited to those pre-selected points. The second approach uses a full coupling between NSMB and Senkin, making it possible to conduct reactive mixture calculations accounting for both the flow field and the chemical reactions. However, this coupling had to be extended for turbulent chemistry by implementing a correction velocity, as the turbulent Schmidt number is calculated per species, in order to grant the mass conservation. This was done similar an approach for the laminar case explained in literature, such as [12]. The correction velocity is stated below.

$$V_i^c = \sum_{k=1}^{N} \left(\left(\frac{\mu}{Sc} + \frac{\mu_t}{Sc_{k,t}} \right) \frac{\partial \tilde{Y}_k}{\partial x_i} \right) \tag{3}$$

where μ denotes the dynamic viscosity, Sc the Schmidt number, Y the mass fraction (Favre averaged) and x_i the three coordinate axes. The index t indicates turbulent variables and k each of the N number of species. To save calculation time the chemical evolution is only evaluated once the temperature in a particular block exceeds a threshold value T_{Senkin}. Only the inert flow field is computed before reaching this temperature. As the chemical reactions involved are very slow at lower temperatures and natural gas does not exhibit any negative temperature coefficient behavior, the temperature was set as high as T_{Senkin} 850 K. The chemical mechanism used, for both the pseudo-zero-dimensional and the coupled approach consists of 55 species and 278 reactions that was proposed by Huang and Bushe [13] based on shock tube experiments with natural gas mixtures at engine-like conditions. As the second approach is very intensive in calculation time – several weeks in our case - it was only tested for the direct comparison to the experimental case.

Results and Discussion

The influence of the variation of the three main parameters, the prechamber wall temperature $T_{wall,prechamber}$, the main chamber wall temperature $T_{wall,main}$ and the initial gas temperature T_{init} on the gas temperature distribution at TDC is shown in Fig. 3. The main chamber wall temperature influences not only the gas temperature in the main chamber but also inside the prechamber. The apparent inconsistent effect of elevated temperature pockets in the main chamber when lowering the wall temperature is probably due to the boundary condition being set as a constant temperature value. Imposing a heat flux might be a better approximation. Looking at the prechamber temperature distribution it is interesting to note that the hot pocket in the beginning of the cone-shaped upper part of the prechamber extends further down the prechamber. This is due to a change in the flow pattern by the lowered wall temperature influencing the recirculation in the prechamber.

The prechamber wall temperature only affects the conditions inside the prechamber leaving the main chamber gas temperature distribution unchanged. It therefore seems to be an appropriate parameter for control of the ignition timing and location as it increases the temperature difference between main and prechamber. The influence of the initial gas temperature finally is the most dominant parameter. An increase of the initial gas temperature by 10 K results in an elevated and in particular more homogeneous temperature distribution inside the prechamber. A further increase of the initial temperature reinforces this effect. The main drawback of increasing the initial gas temperature of course is the rise of temperature level in the main chamber at about the same rate, which raises the risk of auto-ignition in the main chamber.

Based on both the temperature distribution of the base case and geometrical considerations - to cover a relevant part of the TDC volume - 15 cells were chosen and based on their temperature-pressure history chemical calculations following the 0-dimensional approach were conducted.

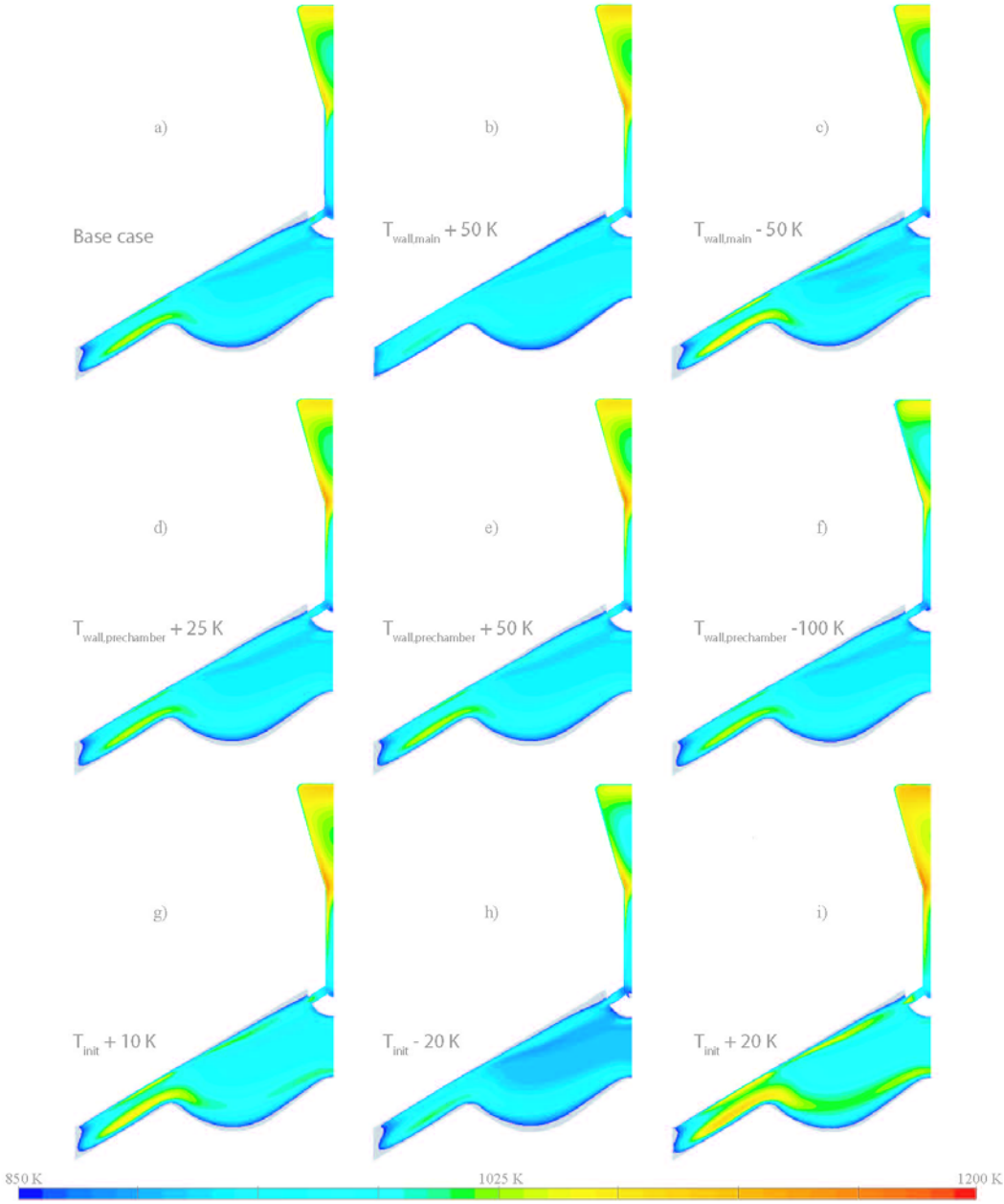

Fig. 3: Temperature distribution for different simulations at top dead centre (TDC).

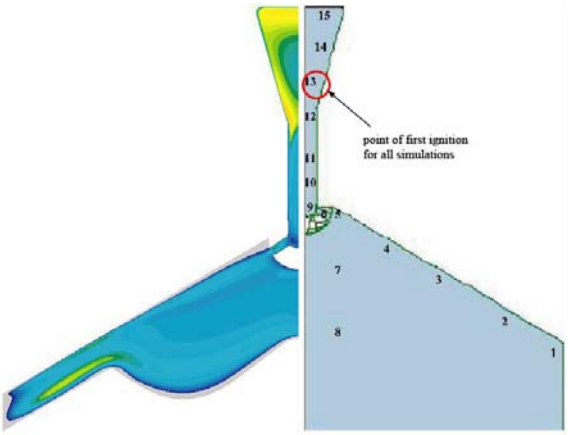

Fig. 4: Temperature distribution of the base case at TDC as basis for the choice of cell elements for the 0-dimensional analysis.

Fig. 4 shows the approximate locations of the 15 cells. It can be shown in all simulations that ignition first started at the lower conical part of the prechamber (Point 13 in Fig. 4). This is consistent with the predicted hot temperature pocket there. Finally, the results of the coupled simulation are shown in Fig. 5, displaying an OH-concentration threshold value in order to illustrate the ignition kernels. Ignition starts at around 18° CA ATDC at the top of the prechamber. The location as well as the timing of the ignition is different from the pseudo-zero-dimensional simulations. It is also evident that the ignition does not occur homogeneously inside the prechamber but the flame propagated down from the location of first ignition at the top of the prechamber.

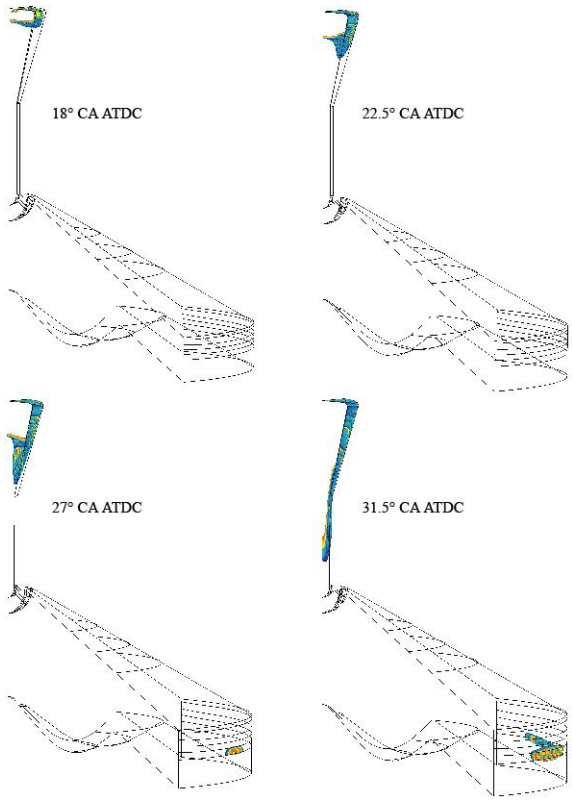

Fig. 5: OH concentration representing the flame front for the coupled calculation.

It also shows that there is a location in the main chamber where the mixture ignites independently from the prechamber in a knock-like fashion. This therefore reinforces results gained from experimental tests indicating independent auto-ignition in the main chamber. In a real engine configuration a location prone to independent ignition would be the relatively hot exhaust valve, which has not been featured in the numerical model. Another point might be the hot tip of the prechamber. The latter location does not seem to be problematic according to the simulation results.

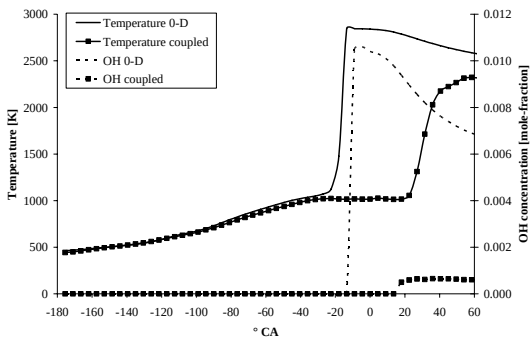

Fig. 6: Temperature and OH concentration profile for pseudo-zero-dimensional and coupled approach.

Fig. 6 shows the temperature evolution and OH concentration at Point 13 for both the zero-dimensional as well as the coupled approach. It clearly demonstrates the difference in ignition time for the two approaches. It should be noted that both approaches are expected to be valid up to the point of ignition only. This is due to the fact that for the zero-dimensional approach the adiabatic coefficient is calculated via a polynomial approximation for the initial gas mixture and therefore is not correct for the burnt gas mixture. For the coupled simulation, as no turbulent flame model is implemented in the code, simulations should only be considered until ignition as well. As the main goal of this study was to locate the ignition kernels, this is sufficient. The difference in ignition timing was investigated in more detail and showed that for the zero-dimensional approach the influence of the start of the chemical calculations on the ignition timing was significant. Superposing the pure CFD temperature and pressure profiles with the chemical calculations with a delay changes the ignition timing drastically. Starting the chemical calculations for example at 67.5° CA BTDC what approximately corresponds to the time when this point reaches the 850 K threshold temperature T_{senkin} in the coupled simulations, the resulting ignition timing for the 0-D approach is at 9° CA BTDC instead of at 18° CA BTDC. This is still different from the result of the fully coupled calculation but could be a possible explanation for the difference between the two approaches. A step-wise decrease of T_{senkin} in the coupled simulation should be done to verify this hypothesis. Another possible reason for the delay of ignition in the coupled approach might simply be convergence problems as during the start of ignition very high temperature and pressure gradients between different cells occur. The density based convergence criterion in NSMB was not fulfilled within the maximum number of inner time steps, propagating a probable non-physical solution for the next time step.

Fig. 7 shows a comparison of the measured and simulated pressure curves for the experimental test case. The pressure data of the CFD simulations is extracted from point 13 and does not represent an integrated value. As the pressure differences over the entire volume are only in the range of a few hundreds of Pascal, this does not represent a significant source of error.

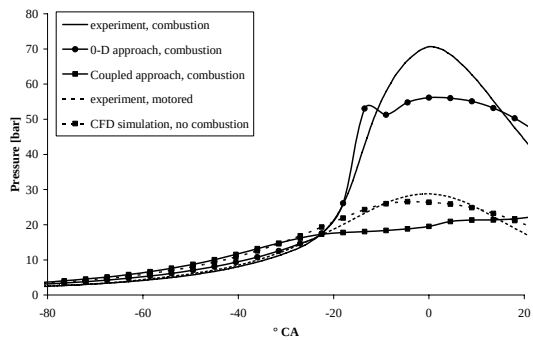

Fig. 7: Pressure curves for experimental case and motored case. Both experimental and simulated curves.

The agreement between the pure CFD simulation and the experimental pressure curve is good. The 0-dimensional approach is in satisfactory agreement

with the measured ignition timing confirming the usefulness of this simplified approach for a rapid evaluation. For the coupled calculation the pressure curve deviates strongly from the other cases. To further investigate the coupled approach it is necessary to use a reduced number of species and reactions in order to conduct simulations within a reasonable time.

Conclusions

The three-dimensional RANS simulation of the engine equipped with a prechamber showed good agreement with the experimental results. It was demonstrated that the location of the first ignition is inside the prechamber but that there is indeed a risk of undesired ignition in the main chamber as was suspected during the experiments. The initial gas temperature is the most influential factor for the ignition timing and can also lead to a more homogeneous temperature distribution inside the prechamber. The heating of the prechamber is an effective control of the gas temperature and therefore the ignition timing. The simulations have also shown that the design of the prechamber is not optimal for the desired homogeneous ignition. It is based on the design of a prechamber for spark ignition where the goal was to minimize the turbulence level at the spark plug location at the top of the prechamber. The goal with the auto-ignition prechamber in contrast is to enhance turbulence and thereby improve the heat transfer from the hot walls. This will be part of further numerical studies aiming for a more homogeneous temperature distribution as well as a maximum temperature difference between main and prechamber.

The pseudo-zero-dimensional approach seems to be a valuable method to scan the calculation domain for regions prone for ignition. Good agreement for the ignition timing could be found for the comparison to an experimental case. The location of first ignition was found to be at the lower end of the diverging conical part of the prechamber, where a hot temperature pocket is induced by the recirculation and stagnation of the gases inside the prechamber. This approach also showed the importance of taking into account the chemical reactions from the very beginning as this drastically influences the ignition timing.

The coupled approach showed different results, which may depend on the numerical resolution as well as on the introduced threshold temperature T_{senkin} for the start of the chemical calculations. In order to further investigate and optimize this approach, it is desirable to reduce the chemical mechanism used as well as to optimize the mesh design in order to speed up the calculations.

Further numerical studies might include the inlet and exhaust valves in order to have a better approximation of the flow conditions and to better assess the possible influence of the hot exhaust valve on independent ignition inside the main chamber. Another important aspect to take into account would be the mixture distribution inside the gas phase as the prechamber is completely filled with exhaust gases at the beginning of the compression stroke, an effect which was not considered in this study.

Acknowledgements

This work is financially supported by the Swiss National Science Foundation (Subsidy Nr. 200020-105487). The availability of the PLEIADES cluster at EPFL, Switzerland for the simulations is gratefully acknowledged by the authors.

References

[1] R.P. Roethlisberger, D. Favrat, Appl. Therm. Eng. 22 (2002) 1217-1229.

[2] R.P. Roethlisberger, D. Favrat, Appl. Therm. Eng. 22 (2002) 1231-1243.

[3] A. Roubaud, D. Favrat, Fuel 84 (2005) 2001-2007

[4] Ordonnance du 16 décembre 1985 sur la protection de l'air (OPair) (state of 23 August 2005)

[5] Q.P. Zheng, H.M. Zhang, D.F. Zhang, Fuel 84 (2005) 1515-1523

[6] M.E. Crane, S.R. King, ASME Trans. JGTP 114 (1992) 466-474

[7] M. Kettner, J. Fischer, A. Nauwerck, J. Tribulowski, U. Spicher, A.Velj, D. Kuhnert, R. Latsch, SAE Paper 2004-01-0035 (2004)

[8] M. Kettner, M. Rothe, A. Velj, U. Spicher, D. Kuhnert, R. Latsch, SAE Paper 2005-01-3688 (2005)

[9] A. Turbiez, A. El Bakali, J. Pauwels, A. Rida, P. Meunier, Fuel 83 (2004) 933-941

[10] J.B. Vos, J. Bohbot, S. Champagneux, J. Cormier, D. Darracq, L. Kozuch, T. Souleres, N. Duquesne. A. Ytterstrom, C. Saint Requier, Y. Le Moine, C. Gacherieu, I. Persson, M. Sillen, NSMB 5.60 User Guide (2005)

[11] R.J. Kee, F.M. Rupley, J.A. Miller, SAND89-8009 (1998)

[12] T. Poinsot, D. Veynante, Theoretical and Numerical Combustion (2005), R.T. Ewards, Philadelphia, USA

[13] J. Huang, W.K. Bushe, Combust. Flame 144 (2006) 74-88